

High-temperature superconductivity on the verge of a structural instability in lanthanum superhydride

Dan Sun^{1*}, Vasily S. Minkov^{2*}, Shirin Mozaffari³, Stella Chariton⁴, Vitali B. Prakapenka⁴, Mikhail I. Erements³, Luis Balicas², & Fedor F. Balakirev¹

1 National High Magnetic Field Laboratory, Los Alamos National Laboratory, NM, US

2 Max-Planck Institut für Chemie, Mainz, Germany

3 National High Magnetic Field Laboratory, Florida State University, Tallahassee, FL, US

4 Center for Advanced Radiation Sources, University of Chicago, Chicago, IL, USA

A possibility of high, room-temperature superconductivity was predicted for metallic hydrogen in the 1960s. However, metallization and superconductivity of hydrogen are yet to be unambiguously demonstrated in the laboratory and may require pressures as high as 5 million atmospheres. Rare earth based “superhydrides” such as LaH₁₀ can be considered a close approximation of metallic hydrogen even though they form at moderately lower pressures. In superhydrides the predominance of H-H metallic bonds and high superconducting transition temperatures bear the hallmarks of metallic hydrogen. Still, experimental studies revealing the key factors controlling their superconductivity are scarce. Here, we report on the pressure and magnetic field response of the superconducting order observed in LaH₁₀. For LaH₁₀ we find a correlation between superconductivity and a structural instability, strongly affecting the lattice vibrations responsible for the superconductivity.

For phonon-mediated superconductors, a high transition temperature necessitates light atomic masses. The lightest atom available to compose a lattice is hydrogen, which forms covalently bonded molecular dimers in ambient conditions. Transforming pure molecular hydrogen with the aid of pressure into a metal with an atomic lattice and into a superconductor has been a long-standing challenge and the subject of contention for the high-pressure community. Yet, chemical pre-compression with certain elements reduces the pressure required for metallization; thus, stable hydrogen-rich phases can be synthesized by the current high-pressure technology. With the discovery of a superconducting transition at the critical temperature $T_c = 203$ K in H₃S¹, the search for hydrogen-rich high-temperature superconductors (HTS) has intensified. A new family of rare-earth hydrides, such as LaH₁₀^{2,3} and YH₉⁴, opened a path for a significant increase in T_c that now approaches room temperature.

While in H₃S the crystal lattice is formed by H-S covalent bonds, LaH₁₀ forms a clathrate-like structure, where each La atom is locked in the center of H₃₂ hydrogen cage. The interatomic distance between hydrogen atoms in LaH₁₀ is close to the H–H distance predicted for atomic metallic hydrogen near $p = 500$ GPa⁵. Due to the short H–H distance and the high hydrogen content, LaH₁₀ can be viewed as ‘doped’ metallic hydrogen. A pronounced isotope effect on T_c when hydrogen is substituted by its heavier isotope deuterium confirmed that the superconductivity in HTS hydrides is induced by electron-phonon interactions⁶. However, there is a dearth of the experimental studies of HTS hydrides due to a very limited number of measurement techniques available at such extreme pressures. Here we explore the features of the lanthanum hydride family over a wide-range of pressures, temperatures, and magnetic fields to better understand the interplay between its structural and superconducting properties. We find that superconductivity in LaH₁₀ is strongly affected by a crystal lattice instability towards symmetry-lowering distortions, a behavior reminiscent of another HTS hydride, namely H₃S, where a dramatic change in the $T_c(p)$ dependence is observed at the structural phase transition^{7, 8, 9, 10}.

Metallic lanthanum reacts readily with excess hydrogen at high pressures and high temperatures yielding clathrate-like superhydrides. We found that the superconducting phase of LaH₁₀ can be prepared from the laser-heated mixture of La and H₂ at a pressure much lower than 150 GPa² or 170 GPa^{3, 11} as reported earlier. Specifically, the X-ray powder diffraction data show that the sample synthesized at 138 GPa for this study is well crystallized and comprised of the dominant $Fm-3m$ LaH₁₀ phase with minor impurities. The impurity phases are attributed to two hexagonal close-packed (*hcp*) phases with $P6_3/mmc$ crystal lattice symmetry and stoichiometry close to LaH₁₀, but with a different c/a ratio: ~ 1.63 for *hcp-I* and ~ 1.48 for *hcp-II* (Fig. 1). Both impurity phases were found previously in various samples prepared via the direct chemical reaction between hydrogen and lanthanum or lanthanum trihydride². The presence of different amounts of *hcp-I* and *hcp-II* phases in samples at ~ 140 - 165 GPa does not distinctly affect the T_c of the superconducting $Fm-3m$ phase which has the highest T_c in the lanthanum-hydrogen system².

Our sample exhibits a narrow superconducting transition towards zero resistance with a high T_c of 243 K at 138 GPa, slightly lower than the maximum T_c of ~ 252 K reported for LaH₁₀ at ~ 165 GPa^{2,3}, in accordance with a “dome-shape” pressure dependence of T_c in the $Fm-3m$ phase of LaH₁₀². The resistivity ρ of LaH₁₀ is estimated to be (0.3 ± 0.1) m $\Omega \cdot$ cm at $T = 300$ K and is higher than the value reported for H₃S¹². The large error is mainly due to the uncertainty of the thickness of the sample.

After a decompression from 138 to 120 GPa some reflections from the ancestral cubic phase became split (Fig. 1) and the T_c dropped to 191 K (Fig. 2). The X-ray diffraction powder patterns of the new distorted phase can be reasonably indexed in the $C2/m$ space group (Fig. 1b, Supplementary Fig. S1). The refined cell parameters and coordinates of the heavier La atoms are in a good agreement with the theoretical prediction for a monoclinic distortion in LaH₁₀ at lower pressures^{13, 14}. Recent calculations of the lowest-enthalpy structures for LaH₁₀ as a function of pressure found the $R-3m$ - to $C2$ - to $P-I$ sequence as a scenario for lattice distortions¹⁵. The structural model of the $C2$ symmetry assumes a subtle shift of the La atoms out from the mirror

plane within the $C2/m$ model, which is about five times smaller than the uncertainty of the refined coordinates for La atom and does not manifest in the experimental X-ray powder patterns.

These structural distortions are reversible, and the $Fm-3m$ phase of LaH_{10} can be restored if the pressure is increased again. The T_c increases gradually with increasing pressure and reaches 241 K at 136 GPa (Figure 2a). We note that the broadening of the superconducting phase transition in Fig. 2a is likely caused by the deterioration of the phase crystallinity during variations of the pressure. However, the stoichiometry is preserved during the phase transition because the volume expansion is in good agreement with the Equation of State (EoS) for LaH_{10} ^{2, 11}. This observation is also in accordance with the calculations, which indicate that the stoichiometry should not change during any crystal distortion in LaH_{10} ^{13, 14, 15}.

The present structural data disagree with the rhombohedral structural distortion scenario towards the $R-3m$ phase of LaH_{10} at 152 GPa as proposed earlier¹¹. Geballe *et al.* studied the structural stability of the $Fm-3m$ phase of LaH_{10} upon decompression from 169 to 27 GPa and found a phase transition that breaks the lattice symmetry into the $R-3m$ phase observed between 152 and 121 GPa, followed by decomposition into a compound with a stoichiometry close to LaH_7 observed from 109 to 92 GPa. With neither Rietveld nor Le Bail refinements of X-ray diffraction patterns provided, the accuracy of the proposed $R-3m$ structural model is questionable. The indexing of the powder diffraction patterns was also aggravated by the poor crystallinity of the sample and the high anisotropic stress induced by the lack of a hydrostatic medium inside the diamond anvil cell (DAC) after heating and subsequent absorption of hydrogen by the tungsten gasket. The uncertainty in pressure estimated using different pressure-markers was as high as 30 GPa, indicating large pressure gradients in samples. Thus, the pressure values were systematically overestimated by 15-20 GPa in the previous study¹¹. Indeed, the lattice volume per La atom in $Fm-3m$ LaH_{10} at 138 GPa (34.3 \AA^3) and $C2/m$ LaH_{10} at 120 GPa (35.4 \AA^3) refined in the present study corresponds to the same volume values in Ref. 11 at 154 GPa and 139 GPa, respectively. Since the fine crystalline sample synthesized here is surrounded by excess hydrogen, which provides a quasi-hydrostatic medium, and the reflections in the X-ray powder pattern are spotty and narrow, the pressure estimate should be more accurate in the present study. Thus, the pressure value of 152 GPa claimed for the beginning of structural distortions in the $Fm-3m$ phase of LaH_{10} in Ref. 11 should be reduced to 135 GPa.

The key parameters of the superconducting phase, including the upper critical field, H_{c2} , and the superconducting coherence length, ξ , for $Fm-3m$ and $C2/m$ LaH_{10} were determined through magnetotransport measurements at the National High Magnetic Field Laboratory. The samples were electrically connected in a van der Pauw configuration (Fig. 2c, inset), making the measurements of both resistivity and Hall effect possible. The LaH_{10} sample under 120 GPa was measured up to 45 T in DC magnetic fields, and the LaH_{10} sample under 136 GPa was measured in a 65 T pulsed magnet.

The magnetoresistance (MR) of LaH_{10} collected at fixed temperatures is shown in Fig. 3. Under a magnetic field the superconducting transitions span over tens of teslas, which correlates with the broadening of the superconducting transition at zero field (Fig. 2a). The normal state MR above H_{c2} is nearly field- and temperature-independent, with a clear kink at the onset of

superconductivity at H_{c2} . For consistency with the prior studies, the H_{c2} 's are taken as the intersection between the straight-line extrapolations of the normal state magnetoresistance and the slope of the superconducting transition in a method similar to the one followed in Ref. 12. The irreversibility field of the high-temperature superconducting phase (H^*) is taken by extrapolating the leading edge of the transition to the horizontal axis (Supplementary Fig. 2). The Hall resistance signal measured above T_c is consistent with the electron-like Fermi surface (Supplementary Fig. 3).

We find that the pressure dependence of T_c in Fig. 2 displays two distinct regions – a low-pressure region characterized by a sharp rise in T_c , and a high-pressure region with a much more moderate dome-like $T_c(p)$ dependence, with a clear boundary between the two regions at 135 GPa. This distinct shape in $T_c(p)$ in LaH₁₀ closely resembles the T_c variation first discovered in the hydride H₃S, and it is explained by the change of the crystalline structure^{7, 9, 10}. At high pressures, the H atoms in H₃S occupy symmetric positions between S atoms ($Im-3m$ symmetry group), but the H sub-lattice distorts slightly in the $R3m$ space group as the pressure is decreased. A sharp, but continuous drop in T_c is observed as H₃S undergoes a structural transition. Multiple distorted hydrogen arrangements from a high-symmetry $Fm-3m$ phase are predicted for LaH₁₀ as well¹⁵. One of the predictions reports a stable LaH₁₀ $Fm-3m$ phase at high pressures, with symmetric H positions and a T_c of 259 K at 170 GPa. The drop in pressure is predicted to stabilize a distorted $R-3m$ phase of LaH₁₀, with $T_c = 203$ K at 150 GPa¹⁴. A $T_c \sim 229-245$ K was calculated for the $C2/m$ phase, although the calculations were performed for $p = 200$ GPa, which is substantially higher than the values presented here¹³.

A likely explanation for the sharp change in the dependence of T_c with pressure below 135 GPa, is a structural phase transition in LaH₁₀. The lack of a discontinuous jump in T_c in LaH₁₀ and in H₃S^{7, 9} points to a continuous symmetry-lowering lattice distortion or a phase transition of the second-order. Although a possible first-order transition was also proposed for H₃S¹⁰, it would result in a discontinuous jump in T_c , which we do not observe.

A higher-symmetry crystal structure transformation into a lower-symmetry phase is governed by phonon softening when the frequency of the collective atomic movement approaches zero. Such a drastic change in phonon modes often has a profound effect on the phonon-mediated superconducting order. A boost in T_c due to phonon softening in the vicinity of a structural transition has been reported in a number of superconducting families, ranging from Sn nanostructures¹⁶, A15 compounds¹⁷, intercalated graphite¹⁸, ternary silicides¹⁹, and even some elements under pressure^{20, 21}. A symmetry-lowering distortion in the H sub-lattice in LaH₁₀ is driven by softening of some of the H-H phonon modes, leading to stronger electron-phonon interaction in the $Fm-3m$ phase, which is characterized by a coupling constant $\lambda = 2 \int_0^\infty \alpha^2 F(\omega) \omega^{-1} d\omega$, where ω is phonon frequency, $F(\omega)$ is the phonon density of states, and α^2 is an average square electron-phonon matrix element. While the light atomic mass of hydrogen is a necessary requirement for phonon-coupled HTS, the T_c is also strongly affected by λ ^{22, 23}, with a peak in T_c predicted for large $\lambda \sim 2-2.5$, which should occur in the close proximity to lattice instability in HTS hydrides²⁴.

Upper critical field measurements in H₃S HTS hydride have independently verified a large $\lambda \sim 2$ ¹². We find a substantially larger H_{c2} for LaH₁₀ and determined that magnetic fields of the order of 100 T will be required to distinguish between a strongly-coupled scenario with a large λ and more commonly employed Werthamer-Helfand-Hohenberg (WHH) model derived in a weakly-coupled limit, $\lambda \ll 1$ ²⁵. To extract the key superconducting properties of LaH₁₀ and explore the effects of the structural transition on superconductivity, we fit the temperature dependence of H_{c2} to WHH (Figure 4 and Table 1). WHH model fits well with our data up to 60 T, our upper measurement limit. The WHH model considers the combined effects of magnetic field on the orbital motion and on the spin of electrons: $H_{c2}^{-2} = H_{c_{orb}}^{-2} + H_{c_p}^{-2}$, where $H_{c_{orb}}$ and H_{c_p} are the orbitally-limited and spin-limited (Pauli) critical fields, respectively. We obtain $H_{c_p}(0)$ values of 352 T at 120 GPa and 457 T at 136 GPa. $H_{c_p}(0)$ values are by a factor of ~ 3 larger than $H_{c2}(0)$ values listed in Table 1, indicating predominantly orbital-limited upper critical field in HTS LaH₁₀, analogous to H₃S¹².

The WHH fit provides a reasonable estimate of the superconducting coherence length $\xi = \sqrt{\Phi_0/2\pi H_{c2}}$, where Φ_0 is the magnetic flux quantum. There is a significant drop in T_c in the distorted phase of LaH₁₀ at 120 GPa when compared to the LaH₁₀ sample at 136 GPa. Surprisingly, $H_{c2}(0)$ only drops by a small amount and, thus, $\xi(0)$ remains nearly unchanged. ξ is linked to both T_c and the Femi velocity v_F : $\xi = 0.18 \hbar v_F / k_B T_c$ within BCS theory⁶, but the $\xi \sim v_F / T_c$ rule should remain valid for other models, thus signaling a decreased v_F in the $C2/m$ phase at 120 GPa when compared to that $Fm-3m$ phase at 136 GPa. The onset of the lattice distortion is expected to strongly affect the electron dispersion, e.g. via the flattening of the bands at the new Brillouin zone boundaries, which may lead to a drop in v_F so that ξ and H_{c2} remain high despite the drop in T_c in $C2/m$ phase.

In conclusion, we have measured the properties of LaH₁₀ HTS superhydride as a function of pressure, temperature, and high magnetic fields. We find evidence for a pressure-induced structural transition in LaH₁₀ at $p_c = 135$ GPa, resulting in a steep, but continuous decrease in $T_c(p)$ below p_c . A likely mechanism for the structural instability is phonon softening and a gradual distortion of the lattice, in common with another HTS hydride H₃S. We established key superconducting quantities of superhydrides under high magnetic fields, including upper critical fields and coherence lengths. We find that the drop in the Femi velocity in LaH₁₀ is consistent with the Brillouin zone changes induced by the distortions. The proximity of peak T_c and symmetry-lowering structural transition, which is now experimentally established for at least two HTS hydride families, indicates that tuning of the soft phonon modes should be viewed as one of the main pathways for maximizing T_c in hydride superconductors.

ACKNOWLEDGMENTS

The work performed at the National High Magnetic Field Laboratory is supported by the National Science Foundation Cooperative Agreement No. DMR-1644779, and the State of Florida. L. B. is supported by the Department of Energy, Basic Energy Sciences through award DE-SC0002613. The synchrotron X-Ray diffraction data were collected at GeoSoilEnviro CARS (The University of Chicago, Sector 13), Advanced Photon Source (APS), Argonne National Laboratory (USA).

GeoSoilEnviro CARS is supported by the National Science Foundation-Earth Sciences (EAR-1634415) and Department of Energy-GeoSciences (DE-FG02-94ER14466). This research used resources of the Advanced Photon Source, a U.S. Department of Energy (DOE) Office of Science User Facility operated for the DOE Office of Science by Argonne National Laboratory under Contract No. DE-AC02-06CH11357. M.I.E acknowledge great support from Max Planck Society.

AUTHOR CONTRIBUTION

D.S., V.S.M. and F.F.B. designed the research and wrote the paper; V.S.M. prepared the samples, collected synchrotron X-Ray diffraction data, performed electrical transport measurements without external magnetic field and processed the structural data; D.S., F.F.B., S.M., L.B. and M.I.E. performed electrical transport measurements under external magnetic fields and processed the data; D.S., F.F.B., S.C. and V.B.P. assisted with the synchrotron X-ray diffraction experiments; M.I.E. designed the diamond anvil cell. All authors contributed to writing the paper. D.S. and V.S.M. contributed equally to this work.

DATA AVAILABILITY STATEMENT

The data that support the findings of this study are available from the corresponding author upon reasonable request.

ADDITIONAL INFORMATION

Supplementary Information is available for this paper. Correspondence and requests for materials should be addressed to D.S. and F.F.B..

References

- [1] Drozdov, A. P., Eremets, M. I., Troyan, I. A., Ksenofontov, V. & Shylin, S. I., "Conventional superconductivity at 203 Kelvin at high pressures in the sulfurhydride system." *Nature* **525**, 73-76 (2015).
- [2] Drozdov, A. P., Kong, P., Minkov, V., Besedin, S., Kuzovnikov, M., Mozaffari, S., Balicas, L., Balakirev, F., Graf, D., Prakapenka, V., Greenberg, E., Knyazev, D. A., Tkacz M. & Eremets, M. I. "Superconductivity at 250 K in lanthanum hydride under high pressures." *Nature* **569**, 528-531 (2019).
- [3] Somayazulu, M., Ahart, M., Mishra, A., Geballe, Z., Baldini, M., Meng, Y., Struzhkin V., & Hemley R. "Evidence for superconductivity above 260 K in lanthanum superhydride at megabar pressures." *Phys. Rev. Lett.* **122**, 027001 (2019).
- [4] Kong, P., Minkov, V., Kuzovnikov, M., Besedin, S., Drozdov, A., Mozaffari, S., Balicas, L., Balakirev, F., Prakapenka, V., Greenberg, E., Knyazev D., & Eremets, M. I. "Superconductivity up to 243 K in yttrium hydrides under high pressure." Preprint at <http://arXiv.org/abs/1909.10482> (2019).

- [5] Liu, H., Naumov, I. I., Hoffmann, R., Ashcroft, N. W. & Hemley, R. J. "Potential high- T_c superconducting lanthanum and yttrium hydrides at high pressure." *Proc. Natl. Acad. Sci.* **114**, 6990-6995 (2017).
- [6] Bardeen, J., Cooper, L. N., & Schrieffer, J. R. "Theory of superconductivity." *Phys. Rev.* **108**, 1175 (1957).
- [7] Einaga, M. et al. "Crystal structure of the superconducting phase of sulfur hydride." *Nat. Phys.* **12**, 835-838 (2016).
- [8] Goncharov, A. F., Lobanov, S. S., Prakapenka V. B. & Greenberg, E. "Stable high-pressure phases in the H-S system determined by chemically." *Phys. Rev. B* **95**, 140101 (2017).
- [9] Minkov, V. S., Prakapenka, V. B., Greenberg E. & Eremets, M. I. "Boosted critical temperature of 166 K in superconducting D_3S synthesized from elemental sulfur and hydrogen." *Angew. Chem. Int. Ed.* **59**, (2020).
- [10] Gor'kov, L., & Kresin, V. "Sulfur Hydrides: Phase Diagram and the Transition into the Record-High T_c State." *J. Supercond. Novel Magn.* **31**, 1-5 (2018).
- [11] Geballe, Z. M. et al. "Synthesis and stability of lanthanum superhydrides." *Angew. Chem.* **130**, 696-700 (2018).
- [12] Mozaffari, S., Sun, D., Minkov, V., Drozdov, A., Knyazev, D., Betts, J., Einaga, M., Shimizu, K., Eremets, M., Balicas L., & Balakirev, F. "Superconducting phase diagram of H_3S under high magnetic fields." *Nat. Commun.* **10**, 2522 (2019).
- [13] Liu, H. et al. "Dynamics and superconductivity in compressed lanthanum superhydride." *Phys. Rev. B* **98**, 100102 (2018).
- [14] Kruglov, I. et al. "Superconductivity of LaH_{10} and LaH_{16} polyhydrides," *Phys. Rev. B* **101**, 024508 (2020).
- [15] Errea, I. et al. "Quantum crystal structure in the 250-kelvin superconducting lanthanum hydride." *Nature* **578**, 66-69 (2020).
- [16] Houben, K. et al. "The influence of phonon softening on the superconducting critical temperature of Sn nanostructures." *Sci Rep.* **10**, 5729 (2020) .
- [17] Testardi, L. R. "Structural instability and superconductivity in A-15 coraipounds," *Rev. Mod. Phys.* **47** (1975).
- [18] Gauzzi, A. et al. "Enhancement of Superconductivity and Evidence of Structural Instability in Intercalated Graphite CaC_6 under High Pressure." *Phys. Rev. Lett.* **98**, 067002 (2007).
- [19] Kuroiwa, S. et al. "Soft-phonon-driven superconductivity in $CaAlSi$ as seen by inelastic x-ray scattering." *Phys. Rev. B* **77**, 140503 (2008).

- [20] Mauri, F. et al. "Phonon Softening and Superconductivity in Tellurium under Pressure." *Phys. Rev. Lett.* **77**, 1151 (1996).
- [21] Suzuki, N. & Otani, M. "The role of the phonon anomaly in the superconductivity of vanadium and selenium under high pressures." *J. Phys.: Condens. Matter* **19**, 125206 (2007).
- [22] McMillan, W. L. "Transition Temperature of Strong-Coupled Superconductors." *Phys. Rev. B* **167**, 331 (1968).
- [23] Allen, P. B. & Dynes, R. C. "Transition temperature of strong-coupled superconductors reanalyzed," *Phys. Rev. B* **12**, 905 (1975).
- [24] Quan, Y., Ghosh, S. S., & Pickett, W. E. "Compressed hydrides as metallic hydrogen superconductors." *Phys. Rev. B* **100**, 184505 (2019).
- [25] Werthamer, N. R., Helfand, E., & Hohenberg, P. C. "Temperature and purity dependence of the superconducting critical field H_{c2} III. electron spin and spin-orbit effects." *Phys. Rev.* **147**, 295, (1966).

Table 1. Summary of samples properties and the associated WHH fit parameters: the critical temperature, the upper critical field at $T=0$, coherence length at $T=0$, BCS Fermi velocity, and the slope of H_{c2} at the critical temperature.

Sample structure	p (GPa)	T_c (K)	$H_{c2}(T=0)$ (T)	$\xi(T=0)$ (nm)	v_F ($\times 10^5$ m/s)	$dH_{c2}/dT _{T_c}$ (T/K)
$C2/m$ LaH ₁₀	120	189	133.5	1.57	2.17	-1.12
$Fm-3m$ LaH ₁₀	136	246	143.5	1.514	2.77	-0.83

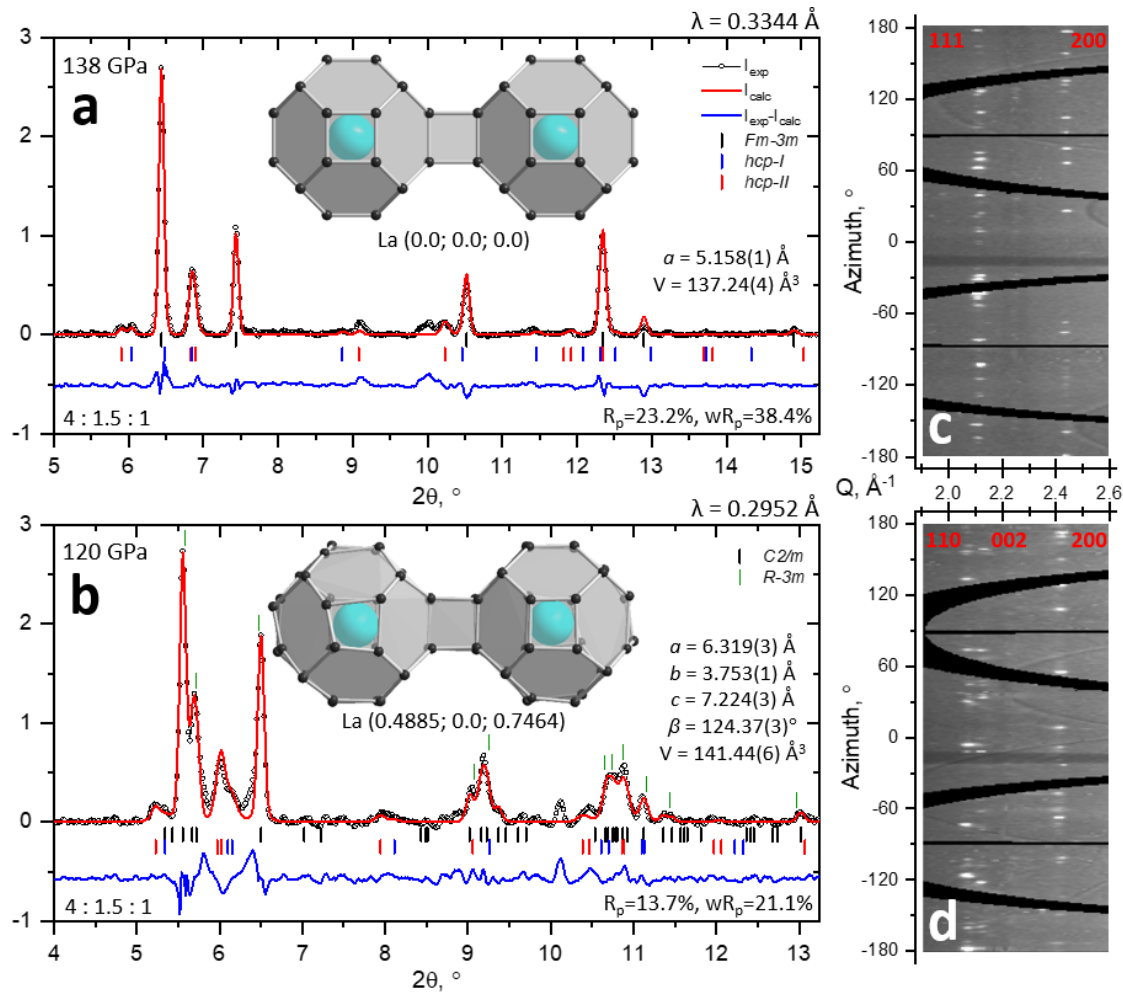


Figure 1. Structural data for LaH₁₀ synthesized from La and excess H₂. **a, b**, Rietveld refinement for *Fm-3m* phase of LaH₁₀ at 138 GPa and *C2/m* phase of LaH₁₀ at 120 GPa, respectively. The peaks originating from the *hcp-I* ($a=3.668(4) \text{ \AA}$; $c=5.914(11) \text{ \AA}$; $V=68.9(1) \text{ \AA}^3$) at 138 GPa and *hcp-II* ($a=3.750(3) \text{ \AA}$; $c=5.561(7) \text{ \AA}$; $V=67.7(1) \text{ \AA}^3$) at 138 GPa impurity phases having *P6₃/mmc* symmetry and LaH₁₀ stoichiometry are indicated through blue and red dashes, respectively. Green dashes corresponding to reflection positions in the *R-3m* structural model ($a=3.73(1) \text{ \AA}$; $c=8.89(1) \text{ \AA}$; $V=107.2(2) \text{ \AA}^3$), hardly fit the experimental powder pattern and are significantly shifted from the observed maxima (Supplementary Fig. S1). The refined ratio between the main and the impurity phases is provided in the left bottom corner of each figure. The main structural building block, two connected LaH₃₂ polyhedra, for each phase are shown in the middle inserts. Large blue and small black spheres correspond to La and H atoms, respectively. H atoms were placed in the calculated positions using predicted structural models¹³. **c, d**, The original X-ray diffraction powder patterns at 138 GPa and 120 GPa, respectively. New reflections appear at 120 GPa due to the monoclinic distortions. These reflections are absent in *Fm-3m* lattice at 138 GPa.

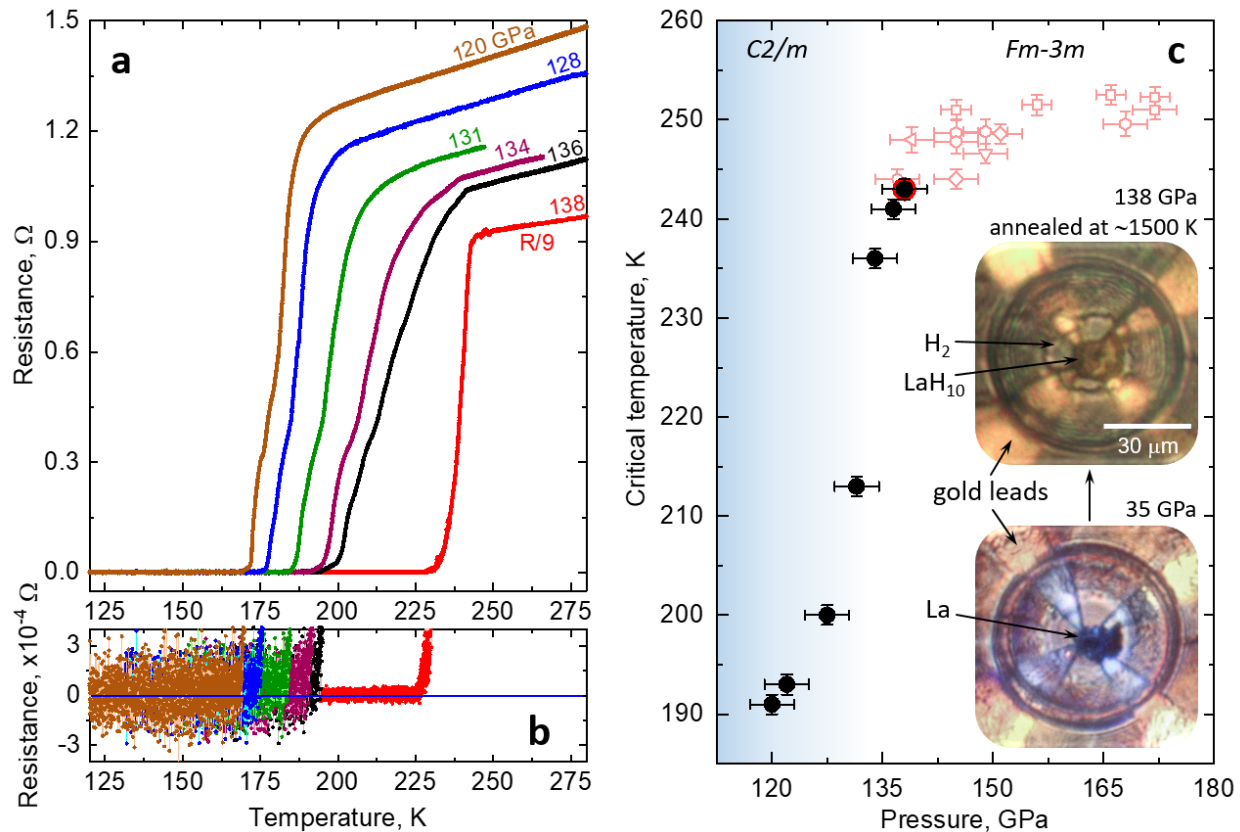


Figure 2. The superconducting transitions in LaH₁₀. **a, b**, The electrical resistance in LaH₁₀ after the synthesis at 138 GPa (red curve), after decompression down to 120 GPa (brown curve), and upon a gradual increase in pressure from 120 to 136 GPa (blue, green, purple, and black curves). The data measured at 138 GPa are divided by 9 for better presentation. **c**, Pressure dependence of T_c in LaH₁₀ measured in the present study (black symbols), and from a prior study² (open red symbols). Inserts: photos of the DAC loaded with a La flake and after the synthesis of LaH₁₀ through laser-assisted heating.

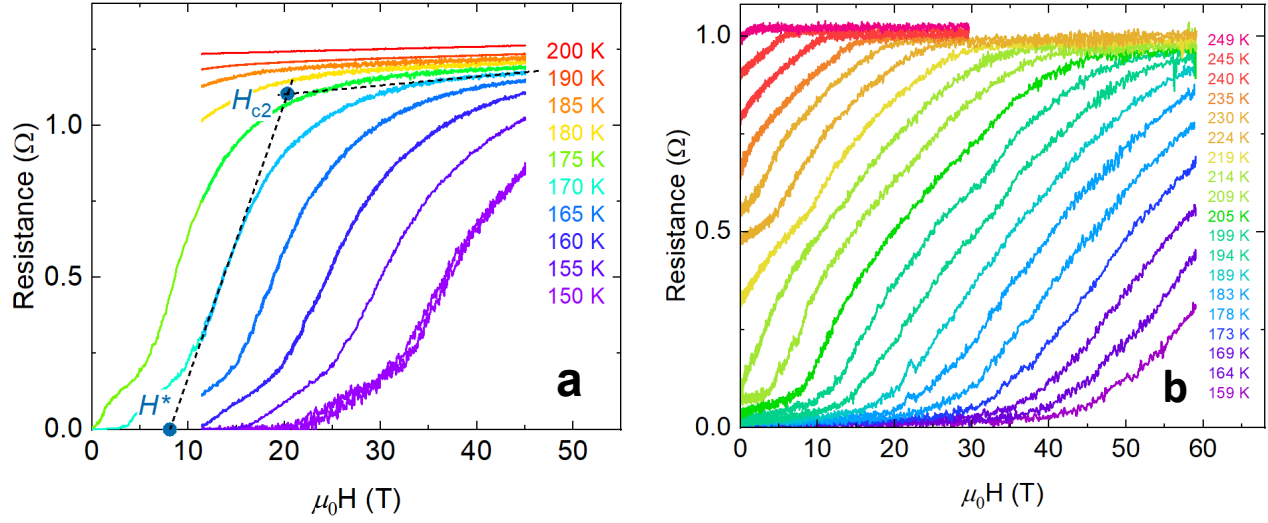


Figure 3. Field dependence of the resistance of LaH₁₀ at different temperatures. **a**, DC field measurements for the *C2/m* phase of LaH₁₀ at 120 GPa. Two dashed lines extrapolate the slope of the high-temperature superconducting transition (left line) towards the asymptotic trace representing the high field normal state magnetoresistance (right line) at 170 K, respectively. The intersection between two lines provides an estimation of the upper critical field (H_{c2}). The intersection of the first line with horizontal axis indicates the irreversibility field (H^*) for the high temperature superconducting phase. **b**, Pulsed field measurements for the *Fm-3m* phase of LaH₁₀ at 136 GPa. Both DC and pulsed field traces were recorded under isothermal conditions and no eddy-current generated Joule heating due to the sweeping of the field was detected.

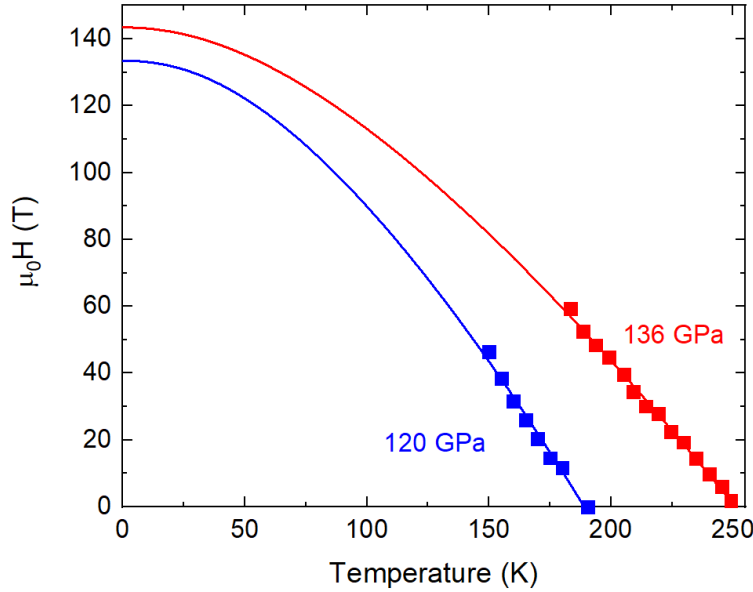


Figure 4. Fits of the superconducting upper critical H_{c2} to the Werthamer-Helfand-Hohenberg (WHH) formalism. Red and blue squares denote the loci of H_{c2} of LaH_{10} at 136 GPa and 120 GPa, respectively. Lines of the same color are the WHH fits to the experimental data.

Methods

Diamond anvil cell

The samples of LaH_{10} were synthesized *in situ* in specially designed miniature diamond anvil cells with a maximum diameter of 8.8 mm and a body length of ~ 30 mm¹. The DAC is small enough to fit in the narrow bore of high field DC and pulsed magnets, and is still able to provide a wide-angle optical opening for laser-assisted synthesis and X-ray measurements, and to reach ultra-high pressures up to 200 GPa.

Sample preparation

For the sample synthesis, a small piece of metallic lanthanum (Alfa Aesar, 99.9%) with a lateral dimension of about 10 μm and a thickness of ~ 1 -2 μm was placed in the center of the beveled diamond anvil with a culet size of 35 μm onto the tips of four sputtered leads. Sputtered gold electrodes were thoroughly isolated from the metal rhenium gasket by a protecting layer made from magnesium oxide, calcium fluoride, and epoxy glue mixture. Excess hydrogen (H_2 , 99.999%; D_2 , 99.75%) was introduced in the DAC at a gas pressure of about 150 MPa. After the cell was thoroughly clamped, the sample was pressurized to the desired pressures (138 GPa for La-H) and then heated up to ~ 1500 -2000 K by a microsecond pulse YAG laser to initiate the chemical reaction between reactants. The pressure was estimated from the Raman shift of the stressed diamond edge²⁶ and the vibron of H_2 ²⁷. Both scales indicated the same pressure within an error of ± 5 GPa.

Structure characterization

X-ray diffraction data were collected at the beamline 13-IDD at GSECARS, Advanced Photon Source using $\lambda_1=0.2952 \text{ \AA}$ and $\lambda_2=0.3344 \text{ \AA}$, beam spot size of $\sim 3 \times 3 \text{ \mu m}$, and Pilatus 1M CdTe detector. Typical exposure time varied between 10-300 s. Processing and integration of the X-ray diffraction powder patterns were carried out using the Dioptas software²⁸. Indexing and Rietveld refinement were performed in GSAS and EXPGUI packages^{29, 30}. The coordinates of the heavier lanthanum atoms were refined, whereas H atoms were placed in the calculated positions derived from the theoretically proposed models^{13, 15, 31}. Structural data for the refined phases of LaH₁₀ can be obtained as Crystallographic Information Files from the Cambridge Crystallographic Data Centre via www.ccdc.cam.ac.uk/data_request/cif, on quoting the Deposition Number: 2033292-2033293

Magnetotransport measurements

Zero field electrical resistance was measured through a four-probe technique in van der Pauw geometry with currents ranging from 10^{-4} A at $p = 138 \text{ GPa}$ to 10^{-3} A at $p = 120 - 136 \text{ GPa}$ samples. No apparent effect of the current value on the measured T_c was observed. The electrical measurements were obtained in a warming part of a thermal cycle as it yields a more accurate temperature reading: a sample is warmed up slowly (0.2 K min^{-1}) under nearly isothermal environmental conditions (no coolant flow). The temperature was measured by a Si diode thermometer attached to the DAC with an accuracy of $\sim 0.1 \text{ K}$. T_c was determined at the offset of superconductivity – at the point of apparent deviation in the temperature dependence of the resistance from the normal metallic behavior. The magnetotransport under high magnetic fields was measured in 45T hybrid magnet and in 65 T pulsed magnet at the National High Magnetic Field Laboratory. A copper thermal shield was placed around the DAC during DC field measurements. The thermal shield was heated uniformly to reduce the thermal gradients, and a secondary Cernox thermometer was attached to the DAC gasket for accurate measurements of the sample temperature. There is no observable heating from the ramping of the magnetic field at rates up to 3 T/min. The Hall effect was measured for the sample at 120 GPa above T_c in hybrid DC magnet from 11.5 T to 45 T. Reverse-field reciprocity method was employed to determine Hall resistance R_{xy} ³² because the field direction of the hybrid magnet cannot be reversed during the day shift. A high-frequency (290 kHz) lock-in amplifier technique was employed to measure sample magnetoresistance in 65 T pulsed magnet. 500 μA AC current was applied to the sample, the voltage drop across the sample was amplified by an instrumentation amplifier and detected by a lock-in. No sample heating was observed during $\sim 50 \text{ ms}$ long magnet pulse based on comparisons of up sweep and down sweep resistance traces at different field sweep rates.

Werthamer-Helfand-Hohenberg model

Numerical fit to the Werthamer-Helfand-Hohenberg model for the temperature dependence of $H_{c2}(T)$ defined by orbital and spin-paramagnetic effects in the dirty limit is given by WHH²⁵:

$$\ln\left(\frac{1}{t}\right) = \sum_{\nu=-\infty}^{\infty} \left\{ \frac{1}{|2\nu+1|} - \left[|2\nu+1| + \frac{\bar{h}}{t} + \frac{(\alpha\bar{h}/t)^2}{|2\nu+1| + (\bar{h} + \lambda_{so})/t} \right]^{-1} \right\}$$

where $h = (4/\pi^2)[H_{c2}(T)/T_c(-dH_{c2}/dT)_{T_c}]$, α is the Maki parameter, and λ_{so} is the spin-orbit constant. The Maki parameter for each sample is estimated from the slope of $H_{c2}(T)$ at $T=T_c$: $\alpha = \sqrt{2} H_{c\text{ orb}}/H_{c\text{ p}} \sim -0.52758 dH_{c2}/dT|_{T_c}$ ²⁵.

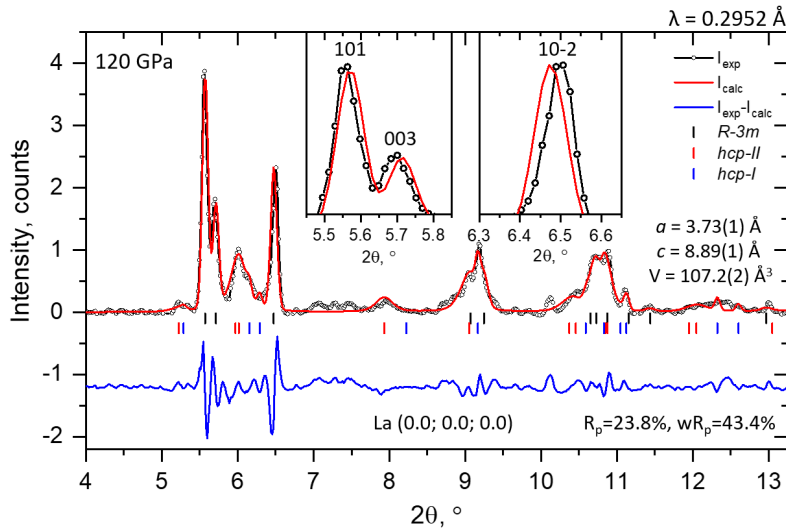
References

- [26] Eremets, M. I. “Megabar high-pressure cells for Raman measurements.” *J. Raman Spectrosc.* **34**, 515–518 (2003).
- [27] Eremets, M. I. & Troyan, I. A. “Conductive dense hydrogen.” *Nat. Mater.* **10**, 927-931 (2011).
- [28] Prescher, C. & Prakapenka, V. B. “DIOPTAS: a program for reduction of two dimensional X-ray diffraction data and data exploration.” *High Press. Res.* **35**, 223–230 (2015).
- [29] Larson, A. C., & Von Dreele, R. B. “General structure analysis system.” *Los Alamos National Laboratory Report LAUR 86-748* (1994).
- [30] Toby, B. H., “EXPGUI, a graphical user interface for GSAS.” *J. Appl. Crystallogr.* **34**, 210–213 (2001).
- [31] Peng, F. et al. “Hydrogen clathrate structures in rare earth hydrides at high pressures: possible route to room-temperature superconductivity.” *Phys. Rev. Lett.* **119**, 107001 (2017).
- [32] Sample, H. H., Bruno, W. J., Sample, S. B., & Sichel, E. K. “Reverse-field reciprocity for conducting specimens in magnetic fields.” *J. of Appl. Phys.* **61**, 1079-1084 (1987).

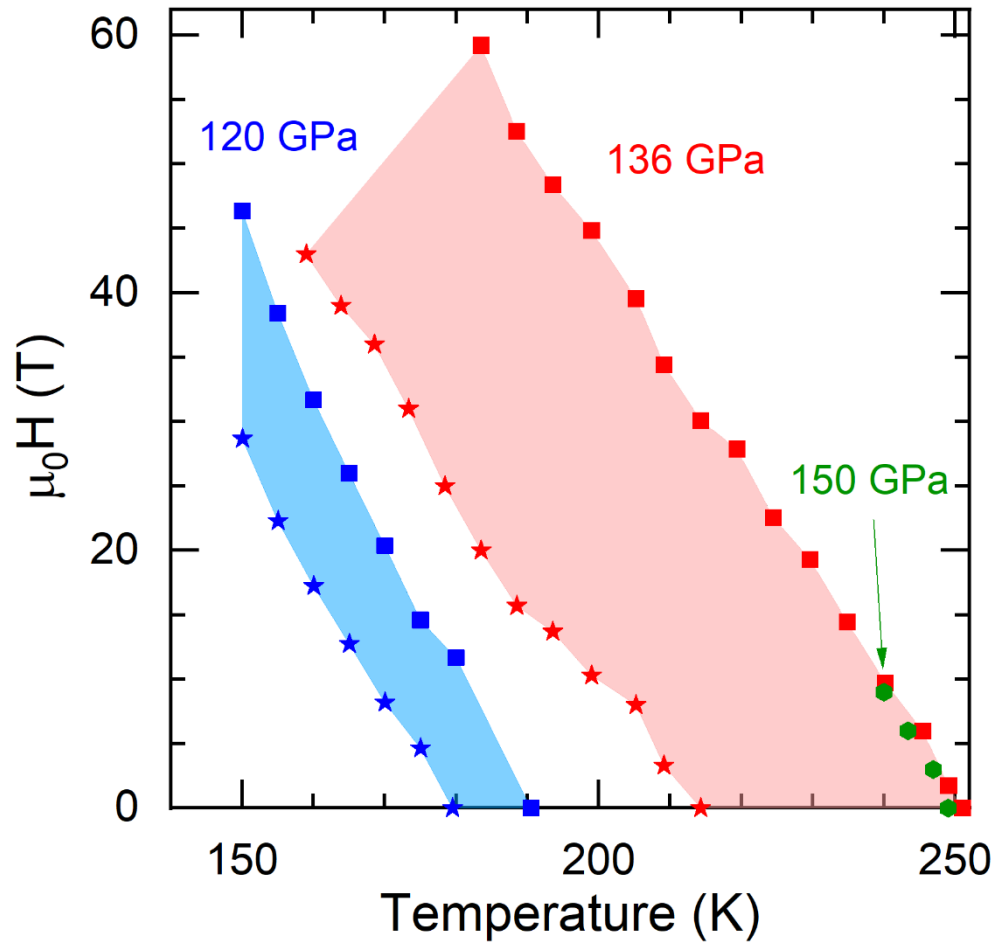
Supplementary Information for

“High-temperature superconductivity on the verge of structural instability in lanthanum superhydride”

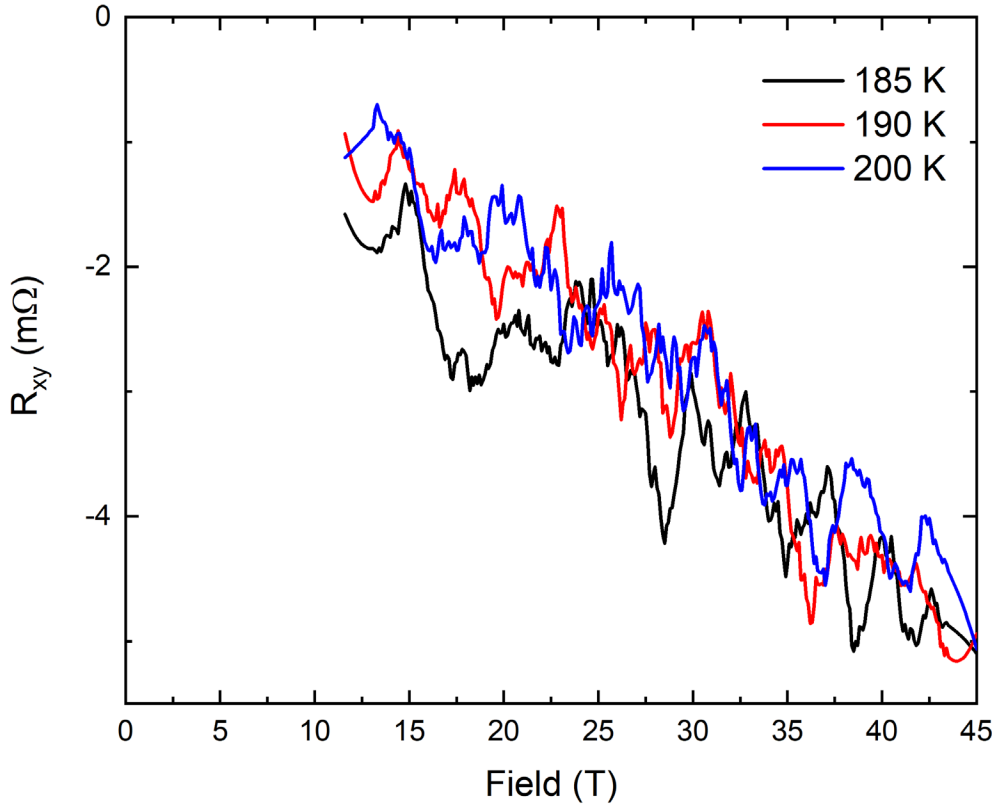
Dan Sun, Vasily S. Minkov, Shirin Mozaffari, Stella Chariton, Vitali B. Prakapenka, Mikhail I. Erements, Luis Balicas & Fedor F. Balakirev



Supplementary Figure 1. The alternative Rietveld refinement for $R-3m$ phase of LaH_{10} at 120 GPa, which demonstrates the worse fitting for the experimental X-ray diffraction powder pattern in comparison with the $C2/m$ structural model. The enlarged inserts show the significant shifts between the calculated positions for the first three 101, 003, and 10-2 reflections in the $R-3m$ structural model from the observed maxima. The refined fitting factors are $R_p = 23.8\%$ and $wR_p = 43.4\%$ and considerably higher than for $C2/m$ model ($R_p = 13.7\%$, $wR_p = 21.1\%$).



Supplementary Figure 2. The upper critical field H_{c2} and the vortex melting field H^* in LaH_{10} . H^* is estimated by extrapolating the leading edge of the transition to horizontal axis and H_{c2} at the offset from the normal state magnetoresistance in $R(H)$ traces from Fig. 3. Stars denote the loci of H^* , and squares denote that of H_{c2} . The blue and red symbols are for LaH_{10} at 120 GPa and 136 GPa, respectively. The green hexagons are the H_{c2} from reference¹. The region of resistive dissipation between H^* and H_{c2} is the so-called vortex liquid state, denoted with red and blue shades. The measurement at 120 GPa has a narrower vortex liquid region while this region becomes wide after pressure is increased to 136 GPa. The upper critical field H_{c2} of the 136 GPa measurement agrees well with the previous measurement up to 9 T in a sample with similar T_c ¹.



Supplementary Figure 3. The Hall resistance in the LaH₁₀ sample at 120 GPa. The Hall effect is measured above T_c in a DC magnet by sweeping the resistive insert field between 11.5 T and 45 T. R_{xy} is linear at all three temperatures, which indicates that the magnetotransport in LaH₁₀ above T_c is dominated by a single electron band. The Hall coefficient R_H value is obtained by taking the slope of R_{xy} and multiplying it by the thickness of the sample. The three measurements yield values $\sim 2.3 \times 10^{-10} m^3/C$. Compared with $0.7 \times 10^{-10} m^3/C$ for H₃S², this R_H value for LaH₁₀ is 3 times larger. From a simple single band model, the density of electrons is $n = -1/R_H e = 7.2 \times 10^{21} cm^{-3}$. This value would indicate that LaH₁₀ has lower carrier density than H₃S, if one disregards some uncertainty about the actual conductive path within the sample. The temperature variance at this temperature range is small, although the variance may come from the noise in the measurement. We find that the Hall signal is lower than the noise in data collected under pulsed-fields at a pressure of 136 GPa, and thus it is not presented here.

References

- [1] Drozdov, A. P., Eremets, M. I., Troyan, I. A., Ksenofontov, V. & Shylin, S. I., "Conventional superconductivity at 203 Kelvin at high pressures in the sulfurhydride system." *Nature* **525**, 73-76 (2015).
- [2] Mozaffari, S., Sun, D., Minkov, V., Drozdov, A., Knyazev, D., Betts, J., Einaga, M., Shimizu, K., Eremets, M., Balicas L., & Balakirev, F. "Superconducting phase diagram of H₃S under high magnetic fields." *Nat. Commun.* **10**, 2522 (2019).